In vitro and In vivo models for studying endothelial cell development and hereditary hemorrhagic telangiectasia

Gkatzis, K.

Chapter 06

"...the post-arterial capillary network plays a critical role
in the formation of direct AV connections
in HHT2 mutants..."

Interaction between ALK1 signaling and connexin40 in the development of arteriovenous malformations

Konstantinos Gkatzis[1], Jérémy Thalgott[2,3], Damien Dos-Santos-Luis[2,3], Sabrina Martin[2,3], Noël Lamandé[2,3], Marie France Carette[4], Frans Disch[5], Repke J. Snijder[5], Cees. J. Westermann[5], Johannes J. Mager[5], S. Paul Oh[6], Lucile Miquerol[7], Helen M. Arthur[8], Christine L. Mummery[1], Franck Lebrin[2,3]*

1Department of Anatomy and Embryology, Leiden University Medical Center, Building 2, Einthovenweg 20, 2333 ZC Leiden, The Netherlands. 2 CNRS Unité mixte de recherché 7241/INSERM U1050, Center for Interdisciplinary Research in Biology, Collège de France, 11 Place Marcelin Berthelot, 75231 Paris cedex 05,France. 3 MEMOLIFE Laboratory of Excellence and Paris Sciences et Lettres Research University, Paris, France. 4AP-HPTenon Hospital, Department of Radiology, 4, rue de la Chine, 75020 Paris, Sorbonne Universités, UPMC University Paris 6, France. 5St. Antonius Hospital, 3435 CM Nieuwegein, The Netherlands. 6 Department of Physiology and Functional Genomics, College of Medicine, University of Florida, Gainesville, Florida, USA. 7 Aix Marseille Université, CNRS IBDM UMR 7288, Campus de Luminy-Case 907, 13288 Marseille cedex 09, France. 8Institute of Genetic Medicine, Newcastle University, Central Parkway, Newcastle NE1 3BZ, UK.

Objective: To determine the role of Gja5 that encodes for the gap junction protein Connexin40 (Cx40) in the generation of arteriovenous malformations (AVMs) in the Hereditary Hemorrhagic Telangiectasia type 2 (HHT2) mouse model.

Approach and results: We identified GJA5 as a target gene of BMP9/ALK1 signaling pathway in human aortic endothelial cells and importantly found that Cx40 levels were particularly low in a small group of HHT2 patients. We next took advantage of the Acvrl1+/- mutant mice that develop lesions similar to those in HHT2 patients and generated Acvrl1+/-; Gja5EGFP/+ mice. Gja5 haploinsufficiency led to vasodilation of the arteries and rarefaction of the capillary bed in Acvrl1+/- mice. At the molecular level, we found that reduced Gja5 in Acvrl1+/- mice stimulated the production of Reactive Oxygen Species, an important mediator of vessel remodeling. In order to normalize the altered hemodynamic forces in Acvrl1+/-; Gja5EGFP/+ mice, capillaries formed transient arteriovenous shunts that could develop into large malformations when exposed to environmental insults.

Conclusions: We identified GJA5 as a potential modifier gene for HHT2. Our findings demonstrate that Acvrl1 haploinsufficiency combined with the effects of modifier genes that regulate vessel caliber are responsible for the heterogeneity and severity of the disease. The mouse models of HHT have led to the proposal that three events –heterozygosity, loss of heterozygosity and a pro-angiogenic- are necessary for AVM formation. Here, we present a novel three-step model in which pathological vessel caliber and consequent altered blood flow are necessary events for AVM development.

Introduction

Hereditary Hemorrhagic Telangiectasia (HHT) is an autosomal dominant genetic vascular disease that affects 1 in 5000 individuals worldwide [1]. The abnormal vascular structures in HHT result predominantly from mutations in *ENG* (HHT1) [2] or *ACVRL1* (HHT2) [3]. The protein products of these genes are receptors for Transforming Growth Factor-β (TGF-β) and/or Bone Morphogenetic Protein (BMP) expressed in endothelial cells that share functions in signaling [4, 5]. Mutations identified to date represent null alleles that lead to reduced levels of receptor at the cell surface indicating that haploinsufficiency is the predominant underlying mechanism of HHT [6]. Both receptors signal to the downstream effectors Smad1/5/8, second messengers that translocate to the nucleus after activation [6]. Therefore, the primary cause of HHT is considered defective TGF-β/BMP signaling in endothelial cells that may lead to the abnormal vasculature [1].

Clinical manifestations of HHT are evident as multiple vessel abnormalities known as telangiectases in the nose, mouth and gastrointestinal tract. These lesions exhibit focal dilation of post-capillary veins that are susceptible to rupture and hemorrhage because of weak vessel walls and high perfusion pressure. As consequence, recurrent and severe epistaxis and gastrointestinal bleeding are common presentation of the disease; this leads to severe anemia requiring iron supplementation and blood transfusions [7]. Large arteriovenous malformations (AVMs) are also found in major organs. They can cause life-threatening complications, although the majority of AVMs remain asymptomatic [7]. AVMs are arteries and veins that appear to fuse without intervening capillaries, to form a network of direct high flow arteriovenous (AV) shunts [8]. They form at the interface between arteries and veins where the capillary bed normally lies and are thought to arise from smaller lesions such as telangiectasia by progressive vascular remodeling [9]. Typically present at birth in the brain, they may develop and grow over time in the lung and liver, although there is still little direct evidence to support this idea [7]. Nevertheless, the recent development of mouse models for HHT and intravital imaging technologies have provided important insights into the mechanisms of AVM formation [10]. Heterozygous *Eng*$^{+/-}$ and *Acvrl1*$^{+/-}$ mice, which are the closest animal models of HHT in terms of genotype, surprisingly develop a relatively normal vasculature with no major defects during developmental angiogenesis. However, some vascular lesions appear in these mice age but only at very low frequency and in an unpredictable manner. This suggests that additional triggers are needed for AVM development [11-13]. Local homozygous loss of *Eng* or *Acvrl1* gene expression, neoangiogenesis, inflammation and wounding have been implicated triggering AV shunt formation, in accordance with secondary triggers acting as underlying mechanisms. Ectopic expression of Vascular Endothelial Growth Factor (VEGF), the prime angiogenic growth factor, using adeno-associated viruses has been shown to induce cerebrovascular dysplasia in both HHT1 and HHT2 mouse models [14, 15]. Inflammation induces "endoglin protein null" locally [16] that may increase the risk of vascular abnormalities in *Eng*$^{+/-}$ mice [13]. Post-natal homologous loss of the *Eng* or *Acvrl1* gene in endothelial cells leads to the formation of AV shunts resembling those seen in HHT individuals only in sites where angiogenesis is active, supporting an hypothesis that at least three hits - the loss of both *Eng* or *Acvrl1* alleles combined with environmental pro-angiogenic triggers - are necessary for AVM development [10].

How mutations in the *Eng* or *Acvrl1* genes lead to AVM formation is still poorly understood, although recent findings indicate that aberrant angiogenesis may account for the development

of such vessel abnormalities [10]. Although the initial stages of AVM formation occur irrespective of blood flow, this process is further exacerbated by flow [17-19]. High-velocity turbulent arterial blood flow results in dilatation and tortuosity of the downstream veins in the skin of mice harboring homologous deletion of *Acvrl1* [17] and promotes mural cell coverage of AVMs in *Eng-iKO* mice [18]. In *Zebrafish*, ALK1 acts downstream of blood flow to limit the number of endothelial cells maintaining the vessel caliber. In agreement, arteries of *Zebrafish* harboring *alk1* mutations deliver a greater blood volume to the downstream vessels that in turn adapt by enlarging and retaining AV connections that are normally transient during angiogenesis in order to normalize hemodynamic forces. This vessel remodeling seems to represent a normal adaptive response to increased blood flow [19]. It is not known how ALK1 regulates arterial vessel caliber. Two flow responsive genes, *cxcr4a* and *edn1*, have been proposed to act downstream of ALK1 to control vessel diameter. These genes encode a pro-angiogenic chemokine receptor and a vasoconstrictive peptide respectively, although additional experiments are required to establish their functions during AVM development in HHT [19, 20]. Here, we describe cooperation between ALK1 and connexin40 (Cx40) in the regulation of blood vessel caliber. The study revealed that reduced expression of Cx40 results in enlargement of the arterial vessels in HHT2 mice and that consequent altered blood flow precipitates flow-dependent adaptive responses involving rarefaction of the capillary network and the formation of direct AV connections. This cooperation is sufficient to trigger AV shunt formation during active angiogenesis and upon additional environmental insult, which resembles vascular lesions seen in HHT patients. Our data suggest that *GJA5* might be a genetic modifier in HHT2.

Results

BMP9/ALK1 regulates endothelial Cx40 expression

Both circumferential strain and wall shear stress affect endothelial gene expression, so that these mechanical forces can be transduced to biochemical signals that facilitate adaptation to changes in blood flow. As ALK1 expression requires blood flow, it is reasonable to assume that this receptor might lie in a mechano-transduction pathway either upstream or downstream of known mechano-responsive genes. However, these genes need to be identified. Here, we revealed that BMP9 stimulation of Human Arterial Endothelial Cells (HAECs) not only induced expression of *ID1* and *HEY2* (**Fig.1A, B**) common downstream targets of ALK1 and Notch signaling pathways [21] but also strongly stimulated the expression of *GJA5* to levels approximately 20-fold higher than the untreated cells after 24 hours of growth factor addition (**Fig.1C**). BMP9 has been shown to activate ALK1-inducing Smad1/5 phosphorylation in endothelial cells [5]. To examine whether ALK1 controls *GJA5* expression, we analyzed the effect of siRNA-mediated knockdown of ALK1 on BMP9-induced *GJA5* in HAECs. siRNA-mediated downregulation of ALK1 expression was confirmed by quantitative PCR (**Fig.1D**). We validated that Smad1/5 phosphorylation was reduced (Figure 1E) and importantly found that *GJA5* mRNA expression was blocked (**Fig.1F**) when ALK1 was decreased in endothelial cells stimulated by BMP9. Among the endothelial Connexins (Cx), Cx40, which is highly expressed in arterial vessels, is essential for the effective transduction of vasodilatation [22-25].

In sections of human skin biopsies stained for Cx40 and Platelet-Endothelial Cell Adhesion Molecule-1 (PECAM-1) as a marker of endothelial cells (**Fig.1G**), we compared 5 control samples with samples isolated from 4 individuals with HHT2. All of these patients had severe HHT-related nosebleeds: the recurrent epistaxis (often 4 incidents per day) did not improve with the regular Argon plasma treatment or medication like tranexamine acid and N-acetylcysteine. Hemoglobin levels were generally low: for one patient for example they varied from 4.4- 8.0 $mmol.l^{-1}$ over a 5 year period and 56 blood transfusions with monthly iron transfusions were necessary to maintain normal blood levels. This patient was also treated with Thalidomide with benefit but stopped because of neuropathy side effects [26]. Another had recurrent epistaxis particularly at night and was also diagnosed with atrial fibrillation. All four patients underwent a Saunders procedure in which their nasal epithelium was partially replaced by skin of their upper arm because of the severity of their symptoms. The surplus skin from the Saunders surgery was frozen and sectioned for analysis of Cx40 expression by immunofluorescence. Cx40 intensity levels were defined as the ratio of the Cx40 integrated intensity to the vessel surface measured as PECAM-1 positive pixels. Cx40 protein levels were particularly low in HHT2 individuals compared to control biopsies (**Fig.1H**) suggesting that the down regulation of Cx40 expression levels in HHT2 individuals is most probably caused by the fact that the remaining wild-type *ACVRL1* allele is unable to contribute protein for normal vascular functions. Our data support an association between ALK1 signaling and Cx40 expression *in vivo*.

Figure 1

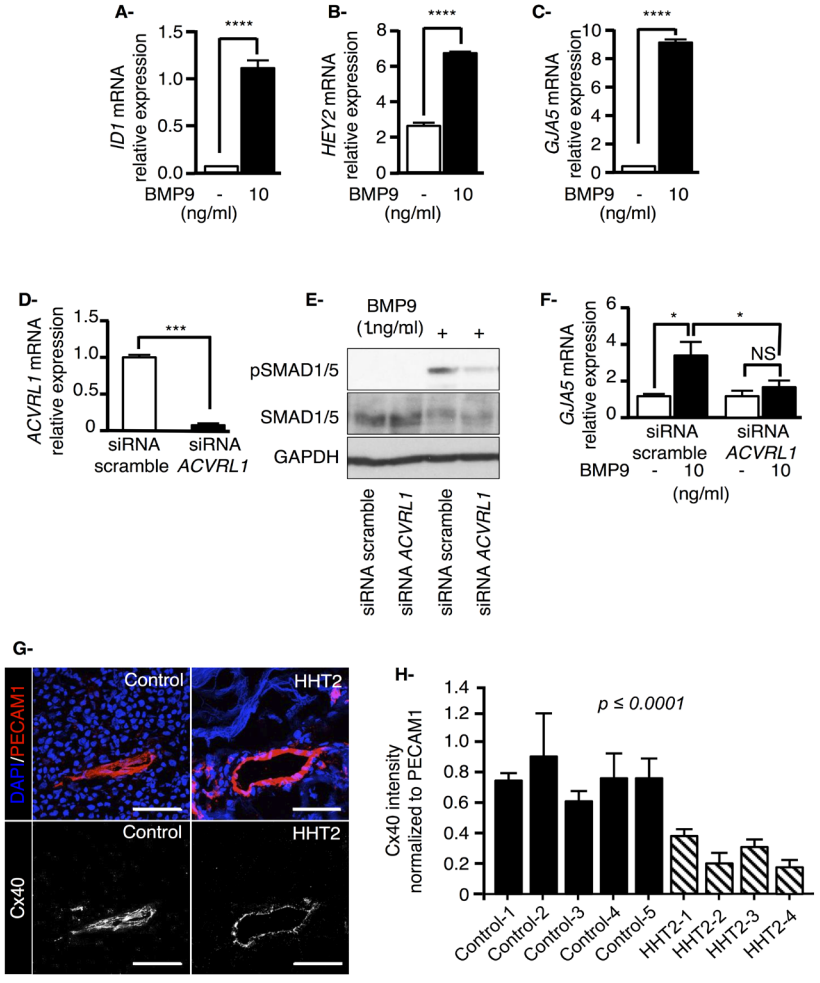

Figure 1: Cx40 is a target gene of BMP9/ALK1 signaling pathway. (A-C) Effect of BMP9 stimulation on ID1 (A), HEY2 (B) and GJA5 (C) mRNA expression in human arterial endothelial cells as determined by quantitative PCR. Results are representative of four independent experiments. (D) The expression of ALK1 in human arterial endothelial cells transfected with siRNA-scramble or siRNA-ACVRL1 was analyzed by quantitative PCR. (E) ALK1 down-regulation inhibits Smad1/5 phosphorylation induced by BMP9. Human arterial endothelial cells transfected with siRNA-scramble or siRNA-ACVRL1 were stimulated with 1 ng/ml of BMP9 for 45 min at 37°C before lysis. Whole-cell extracts were fractionated by SDS-PAGE and blotted. The filter was incubated with pSMAD1/5, SMAD1/5 or GAPDH antibody. (F) SiRNA-ACVRL1 leads to a reduced BMP9-induced GJA5 transcriptional activity. (G) Confocal imaging showing Cx40 protein expression in arterial endothelial cells in skin sections of one representative healthy donor and one representative HHT2 individual. Endothelial cells are stained for PECAM-1 (red) and Cx40 (white) therefore representing arterial vessels. Scale bars: 50µm. (H) Quantification of Cx40-positive surface intensity normalized to PECAM-1 expression in the skin of five healthy donors and four HHT2 individuals. ****P< 0.0001, results from one-way ANOVA that compare means of multiple groups

Reduced levels of Cx40 affect angiogenesis in *Acvrl1*$^{+/-}$ mice

To investigate whether *Acvrl1* and *Gja5* function in the same pathway, we took advantage of the *Acvrl1*$^{+/-}$ mutant mice that develop vascular lesions similar to those in HHT2 patients only at very low frequency and in an unpredictable, age-dependent manner [12]. We generated *Acvrl1*$^{+/-}$*; Gja5*$^{EGFP/+}$ mice that have reduced expression of both genes as validated by quantitative PCR (**Fig.IA, B** in **Data Supplement**), and first examined the neonatal retina. *Gja5*$^{EGFP/+}$ mice are normally viable and fertile without cardiovascular abnormalities [27]. The retinal vasculature of the single or double heterozygotes at postnatal day (P)7 showed a regular alternating pattern of arteries and veins with an intervening capillary network as in control mice (**Fig.2A**). Endothelial tip cells formed filopodial protrusions at the sprouting front of the plexus (**Fig.2A**). However, *Acvrl1*$^{+/-}$ retinas showed excessive angiogenesis with a denser and more highly branched vascular plexus at the front, as previously reported in *Acvrl1-iKO* mutants [28] (**Fig.2A-C**). By contrast, *Acvrl1*$^{+/-}$*; Gja5*$^{EGFP/+}$ mutant mice reproducibly showed reduced angiogenesis with much less dense post-arteriolar capillary plexus (**Fig.2B**) that had fewer branch points (**Fig.2C**). By comparison, capillaries in other regions appeared unaffected (**Fig.2A-C** and **Fig.IIA-C** in **Data Supplement**). Changes in blood flow are known to drive vessel pruning, leading to maturation of the vasculature. Blood flow is generally low during vascular development in the neonatal retina excepted for the arterial segments close to the optic disc and for some of the first arterial branches [29] (Figure IIA in Data Supplement). Interestingly, the reduced number of capillaries was in areas where the blood flow is estimated to be relatively high (**Fig.2A-C** and **Fig.IIA** in **Data Supplement**) [29]. Moreover, mural cell coverage of the arteries was enhanced in *Acvrl1*$^{+/-}$*; Gja5*$^{EGFP/+}$ mutant mice at P7 compared to single heterozygote and wild-type littermates as revealed by staining for asmooth muscle actin (aSMA). Arterioles where only few aSMA positive cells would be normally found at P7 were covered by regular layers of smooth muscle cells, especially near their branch points with the arteries (**Fig.2D-F**). In agreement, *Gja5* expression that correlates with the arterial flow pattern was strongly increased in the arterial vessels of *Acvrl1*$^{+/-}$*; Gja5*$^{EGFP/+}$ P7 mutant mice compared to *Gja5*$^{EGFP/+}$ heterozygous mice as revealed by green fluorescent protein EGFP, suggesting that the blood flow is perturbed in the *Acvrl1*$^{+/-}$*; Gja5*$^{EGFP/+}$ mutant mice (**Fig.2D**).

To eliminate adaptive processes that may occur during embryonic development, in particular those related to blood flow regulation, confounding the analysis, we generated *Acvrl1*$^{Flox/+}$*; cdh5* (PAC)-Cre^{ERT2} (*Acvrl1-iHET*)*; Gja5*$^{EGFP/+}$ mice in which tamoxifen injection of neonatal mice led to efficient reduction of *Acvrl1* mRNA expression to generate *Acvrl1*$^{+/-}$*; Gja5*$^{EGFP/+}$ mice (**Fig.IIIA, B** in **Data Supplement**) [30 31]. Impaired angiogenesis was much more severe in *Acvrl1-iHET; Gja5*$^{EGFP/+}$ mice than in *Acvrl1*$^{+/-}$*; Gja5*$^{EGFP/+}$ mice, with particularly strong inhibition of post-arterial capillary plexus density (**Fig IIID, E** in **Data Supplement**). This confirmed that ALK1 signaling regulates angiogenesis by directly cooperating with Cx40. Thus, reduced Cx40 in HHT2 mice disrupts proper formation of the capillary bed connecting the artery and vein.

Figure 2

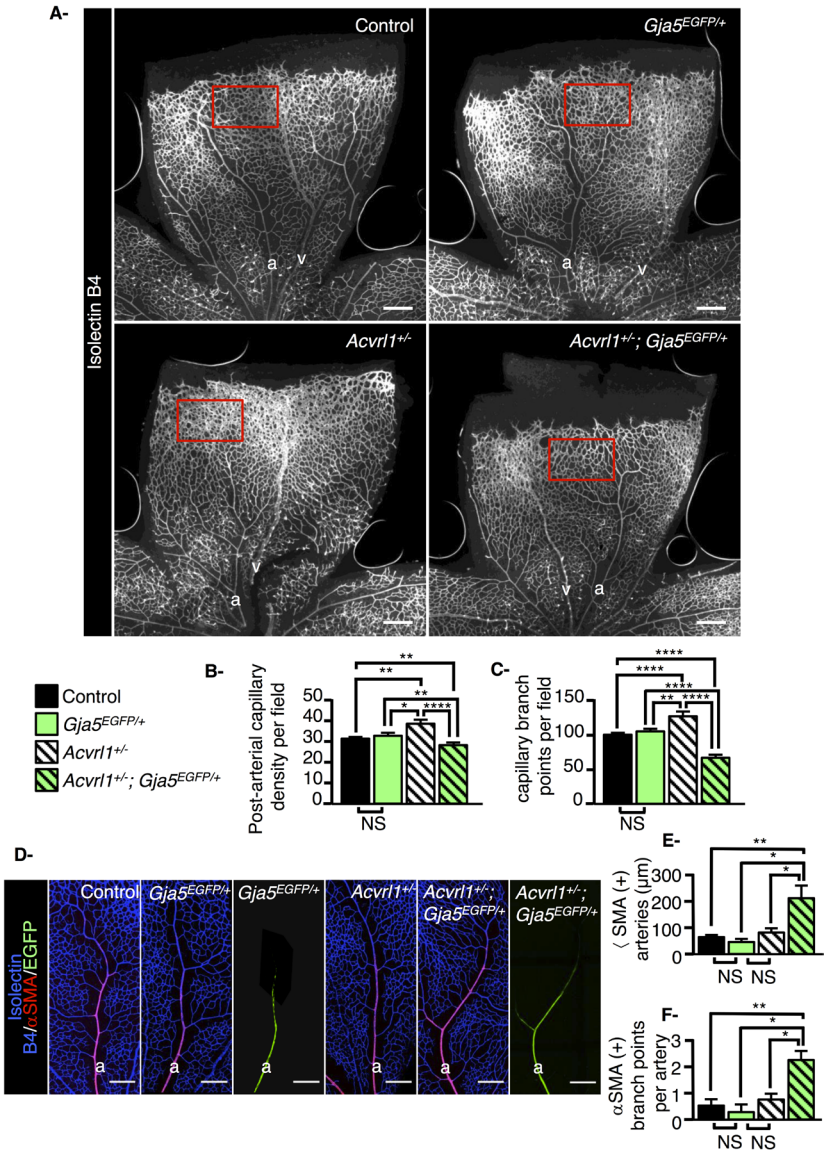

Figure 2: Effect of *Acvrl1* and *Gja5* haploinsufficiency *in vivo*. (**A)** Isolectin B4-stained endothelial cells in retinal vessels in control (n=11), *Gja5*$^{EGFP/+}$ (n=10), *Acvrl1*$^{+/-}$ (n=9) and *Acvrl1*$^{+/-}$; *Gja5*$^{EGFP/+}$ (n=8) mice at P7. The outlined red boxes indicate the areas in which vascular parameters were quantified. (**B-C)** Quantification of post-arterial capillary density **(B)** and number of vessel branch points **(C)** per field. **(D)** Confocal imaging of retinas from control (n=6) *Gja5*$^{EGFP/+}$ (n =4), *Acvrl1*$^{+/-}$ (n=5) and *Acvrl1*$^{+/-}$; *Gja5*$^{EGFP/+}$ (n =7) at P7 stained for Isolectin-B4 that marks endothelial cells (blue) and for aSMA that marks vascular Smooth Muscle Cells (vSMCs) (red). EGFP expression reveals arteries. **(E-F)** Quantification of the aSMA (+) vessel length from the first arterial branch and the number of arterial branch points. All error bars represent s.e.m. $^{*}P< 0.05$, $^{**}P< 0.01$ and $^{****}P< 0.0001$, results from unpaired t test. NS, not significant a, arteries; v, veins. Scale bars, 200µm.

Low levels of Cx40 leads to AV shunts in *Acvrl1*$^{+/-}$ retinas

Because AV shunts are thought to arise from an abnormal capillary bed, we next explored the possibility that reduced levels of Cx40 promote AVM development in *Acvrl1*$^{+/-}$ retinas. We defined vessels ≥ 12.5μm as AV shunts because AV connections of this diameter were not observed in control or single heterozygous mice at P7 (**Fig.3A-D**). AV shunts occurred in 71% (n=14) of the *Acvrl1*$^{+/-}$*; Gja5*$^{EGFP/+}$ P7 mice, but were completely absent in controls, *Acvrl1*$^{+/-}$ or *Gja5*$^{EGFP/+}$ mice. The AV shunts were found to arise from the capillary bed starting at the post-arterial capillary vessels to form enlarged vessels that connected directly to the veins (**Fig.3E**). Similar phenotypes were observed in *Acvrl1-iHET; Gja5*$^{EGFP/+}$ mice with a prevalence of 61% (n=13) (**Fig.IVA** in **Data Supplement**). *Acvrl1-iHET* mice did not develop any AV shunts (**Fig.IVA** in **Data Supplement**). To determine whether the increase in AVM diameter was attributable to increased endothelial cell number, we performed BrdU analysis of isolectin b4-stained vessels. In *Acvrl1-iHET; Gja5*$^{EGFP/+}$ mice, the number of BrdU-labeled endothelial cells was significantly higher than in the other genotypes, particularly in the capillary plexus where AV connections were found (**Fig. IVB** in **Data Supplement**). Moreover, these AV shunts lacked smooth muscle cell coverage (not shown). Because increased mural cell coverage of the AVM has been proposed to be a secondary response to increased blood flow, our data indicated that the AV shunts found in the *Acvrl1*$^{+/-}$*; Gja5*$^{EGFP/+}$ mutant mice at P7 might represent an early stage of AVM formation. Thus, our data are consistent with a primary abnormality at the capillary level and point to vessel enlargement promoting the development of AVM.

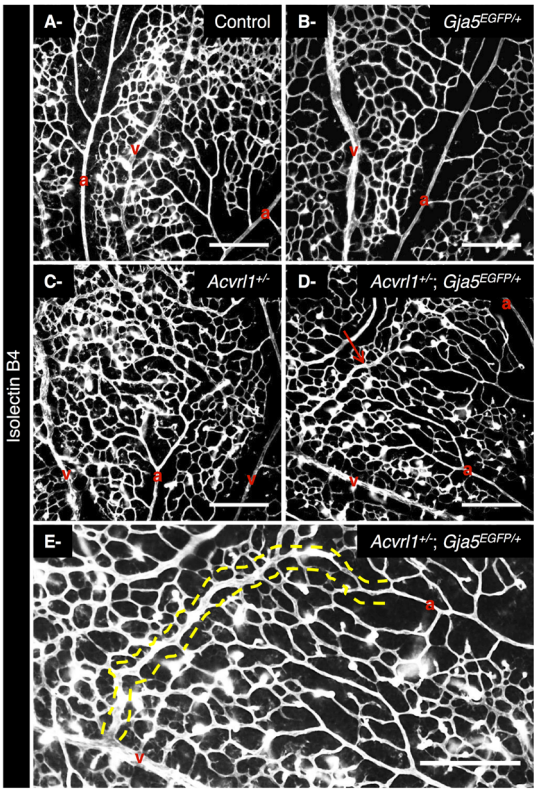

Figure 3: Development of multiple transient arteriovenous connections in *Acvrl1*$^{+/-}$; *Gja5*$^{EGFP/+}$ neonatal retina. (A-D) Confocal images of flat-mounted retinas labeled with isolectin-B4 that reveals the vascular plexus from control, *Gja5*$^{EGFP/+}$, *Acvrl1*$^{+/-}$ and *Acvrl1*$^{+/-}$; *Gja5*$^{EGFP/+}$ at P7. The red arrow indicates a direct connection between an artery and a vein **(E)** Higher magnification of a typical micro-shunt found in *Acvrl1*$^{+/-}$; *Gja5*$^{EGFP/+}$ P7 retinas. Yellow dotted lines delimit the shunt. a, arteries; v, veins. Scale bars, 200μm.

Low levels of Cx40 promote the production of Reactive Oxygen Species and lead to arterial dilation in *Acvrl1*$^{+/-}$ mice

To explore the possibility that the enlargement of capillary-like vessels plays a causal role in the development of AVM, we examined the vasculature in the dorsal ear skin of *Acvrl1*$^{+/-}$*; Gja5*$^{EGFP/+}$ adult mice. This area of skin has recently proven extremely useful for intravital vascular imaging and is widely used to follow AVM development in real time, particularly in wound healing [17]. We stained whole-mounts of 3-month-old mouse ears for PECAM-1 and aSMA (**Fig.4A**). This staining showed that the overall vessel patterning in *Acvrl1*$^{+/-}$*, Gja5*$^{EGFP/+}$ mice was very similar to controls, *Gja5*$^{EGFP/+}$ or *Acvrl1*$^{+/-}$ mice (**Fig.4A**), The vascular network forming a finger-like architecture of larger veins that localize together with arteries that were stained for aSMA (**Fig.4A**). However, the main arteries in the ear skin were reproducibly enlarged in *Acvrl1*$^{+/-}$*; Gja5*$^{EGFP/+}$ adult mice compared to controls, *Acvrl1*$^{+/-}$ or *Gja5*$^{EGFP/+}$ mice (**Fig.4A, B**). Interestingly, the latter seems to occur from early development as seen in the mesencephalic artery of embryonic (E) day 12.5 embryos (**Fig. VA-C** in **Data Supplement**) and in the lung and intestine tissue of E17.5 embryos (**Fig. VD** in **Data Supplement**). We next investigated the *Gja5* expression pattern by following EGFP expression as an indicator of hemodynamic changes and capillary arterialization. In the *Gja5*$^{EGFP/+}$ mice, EGFP expression was restricted to the main arteries and first arteriole branches (data not shown) copying the aSMA staining (**Fig.4A**). By contrast, *Acvrl1*$^{+/-}$*; Gja5*$^{EGFP/+}$ mice showed numerous enlarged pre-arteriolar capillaries that expressed EGFP (not shown) or aSMA (**Fig.4A**) compared to *Gja5*$^{EGFP/+}$ mice. Quantification of the number of branch points and the length of the EGFP (+) vascular networks revealed an arterialization of the blood capillary bed in *Acvrl1*$^{+/-}$*, Gja5*$^{EGFP/+}$ mice (**Fig.4C, D**). We explored how reduced *Gja5* expression affects the arterial vessel functionalities in *Acvrl1*$^{+/-}$ mice. We examined the spontaneous oscillation in tone of the skin arterial vessels (**Fig.4E**) and the ability of the retinal arteries to constrict following an electrical stimulation (**Fig.4F**). The arterial responses of *Acvrl1*$^{+/-}$*, Gja5*$^{EGFP/+}$ mice did not differ from the controls, *Gja5*$^{EGFP/+}$ or *Acvrl1*$^{+/-}$ mice (**Fig.4E, F**) suggesting that the functionalities of the arteries are not defective *per se.* Both *in vitro* and *in vivo* biochemical data have suggested that reduced expression of *Acvrl1* or *Gja5* altered ROS production [32, 33]. To access the potential role of oxidative stress, ROS production was measured by identifying Dihydroethidium (DHE)-positive nuclei in arteries of lung sections of one month-old controls, *Gja5*$^{EGFP/+}$, *Acvrl1*$^{+/-}$ or *Acvrl1*$^{+/-}$*; Gja5*$^{EGFP/+}$ mice. Interestingly, greater DHE-staining was observed in *Acvrl1*$^{+/-}$*; Gja5*$^{EGFP/+}$ mice suggesting higher O_2^- production (**Fig.4G**).

Basal Red Blood Cell (RBC) flow in individual capillaries of *Acvrl1*$^{+/-}$*; Gja5*$^{EGFP/+}$

ROS production and reduced Nitric Oxide (NO) bioavailability have been reported to reduce endothelial cell survival leading to pruning of the microvasculature and contributing to the muscularization of the small arteries [34]. We observed a strong reduction in the density of the capillary bed (**Fig.5A, B**) associated with a slight increase in capillary diameter (**Fig.5C**) in *Acvrl1*$^{+/-}$*; Gja5*$^{EGFP/+}$ mice compared to controls, *Acvrl1*$^{+/-}$ and *Gja5*$^{EGFP/+}$ mice. Capillary rarefaction is associated with local blood flow deregulation. To examine whether this contributed to the vascular phenotype here, we used two-photon microscopy to measure RBC flow with micrometer spatial- and millisecond temporal

Figure 4

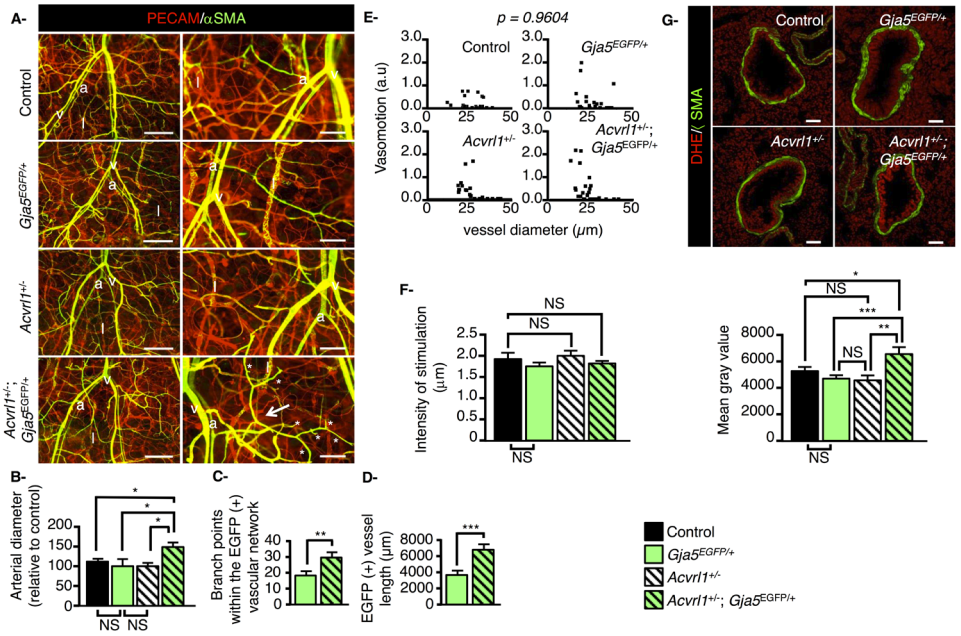

Figure 4: Increased ROS production and arterial dilation in *Acvrl1*$^{+/-}$; *Gja5*$^{EGFP/+}$ mice. (A) Images of whole-mounted ears of control (n=4), *Acvrl1*$^{+/-}$ (n=5), *Gja5*$^{EGFP/+}$ (n=8) and *Acvrl1*$^{+/-}$; *Gja5*$^{EGFP/+}$ (n=12) mice stained with antibodies against PECAM-1 (endothelial cells in red) and aSMA (vSMCs in green) at P60-P90. aSMA reveals arteries. The main arteries and veins are shown in left panels. Scale bars, 500μm. Right panels, higher magnifications of the whole-mount ears reveal an extension of the arterial network in *Acvrl1*$^{+/-}$; *Gja5*$^{EGFP/+}$ mice evident as increase numbers of aSMA (+) vessels. White asterisks indicate arterial branch points. Scale bars, 200μm. **(B)** Quantification of the arterial diameters. **(C-D)** Quantification of the number of branch points and vessel length of the EGFP (+) vascular network. **(E)** The relation between vessel diameter and a vasomotion index defined as the area under the curve for percent spontaneous changes in vessel diameter with a ±5% cutoff threshold, at least n=21 vessel segments from 3 mice per genotype were analyzed. **(F)** Mean intensities that are able to induce the first retinal arterial constriction in controls ($n_{arteries}$ = 32), *Gja5*$^{EGFP/+}$ ($n_{arteries}$ = 28), *Acvrl1*$^{+/-}$ ($n_{arteries}$ = 32) or *Acvrl1*$^{+/-}$; *Gja5*$^{EGFP/+}$ ($n_{arteries}$=30) mice. At least 4 mice of 8-weeks old were analyzed per group **(G)** Increased DHE (red fluorescence) staining in lung sections of 8-week-old *Acvrl1*$^{+/-}$; *Gja5*$^{EGFP/+}$ (n=3) mice versus age-matched control (n=3), *Gja5*$^{EGFP/+}$ (n=3) and *Acvrl1*$^{+/-}$ (n=3) mice. Arterial vessels show more positive nuclei with more intense red fluorescence in *Acvrl1*$^{+/-}$; *Gja5*$^{EGFP/+}$ mice. Scale bars: 50μm. Quantification of the DHE red fluorescence intensity as determined by subtracting the image background from the average gray value within the a-SMA (+) vessels in control (n_{artery}=40), *Gja5*$^{EGFP/+}$ (n_{artery}=62), *Acvrl1*$^{+/-}$ (n_{artery}=35) and *Acvrl1*$^{+/-}$; *Gja5*$^{EGFP/+}$ (n_{artery}=53) lung sections. All error bars represent s.e.m. $^{*}P< 0.05$, $^{**}P< 0.01$, $^{***}P< 0.001$, results from unpaired *t* test or from one-way ANOVA test for multiple group comparison. NS, not significant, a, arteries; v, veins; l, lymphatic vessels.

resolution in individual capillaries [35]. Retro-orbital injection of Red-dextran revealed the vascular architecture of the ear skin as well as individual RBCs, which appeared as shadows flowing in the fluorescent plasma (**Fig.5D**). We used rapid line scans along the capillary axis to determine the instantaneous RBC flow (**Fig.5E**). We analyzed basal RBC flow in at least 29 capillaries that were located in a post-arteriolar position in each genotype and detected all passing RBCs for 20 seconds (**Fig.5F, G**). *Acvrl1*$^{+/-}$*; Gja5*$^{EGFP/+}$ mice showed an increase in basal RBC flow compared to controls, *Acvrl1*$^{+/-}$ and *Gja5*$^{EGFP/+}$ mice most likely reflecting an increase in blood flow (**Fig.5F, G**)

Reduced Cx40 promotes wound-induced AVM formation in *Acvrl1*$^{+/-}$

To explore the possibility that reduced expression of Cx40 might predispose to AVM formation in adult *Acvrl1*$^{+/-}$ mice, we generated punch wounds in the ears of 3-months-old control, *Acvrl1*$^{+/-}$, *Gja5*$^{EGFP/+}$ and *Acvrl1*$^{+/-}$; *Gja5*$^{EGFP/+}$ mice. This type of wound induces environmental stress that triggers AVM formation in homozygous *Acvrl1-iKO* mice [17, 36]. Left ventricular injection of latex blue into the heart was performed 30 days after wounding to visualize AV connections in the skin. As expected, the blue latex did not cross the capillary bed and was retained within the arterial branches in controls or *Gja5*$^{EGFP/+}$ mice (**Fig.6A**). Moreover, *Acvrl1*$^{+/-}$ also showed normal morphology and latex only in arterial branches confirming that three events are required for AVM formation (**Fig.6A**) [10]. By contrast, *Acvrl1*$^{+/-}$; *Gja5*$^{EGFP/+}$ mice showed dilated and tortuous vessels and the latex dye was found in both arteries and veins, indicating the presence of AV shunts (57%, n=7) (**Fig.6A**). Blood vessels away from the wound in *Acvrl1*$^{+/-}$; *Gja5*$^{EGFP/+}$ mice had normal morphology and no AV shunts. We also stained whole mounts of mouse ears for PECAM-1 and aSMA 14 days after wounding. This staining showed that even at this stage *Acvrl1*$^{+/-}$; *Gja5*$^{EGFP/+}$ mice developed abnormal connections between arterioles and enlarged capillary-like vessels that were EGFP (+) forming a nidus (**Fig.6B**). Thus, our data identify *Gja5* as a possible genetic modifier of HHT2 and provide proof-of-concept that genes implicated in blood flow regulation might have important functions during AVM formation.

.

Figure 5

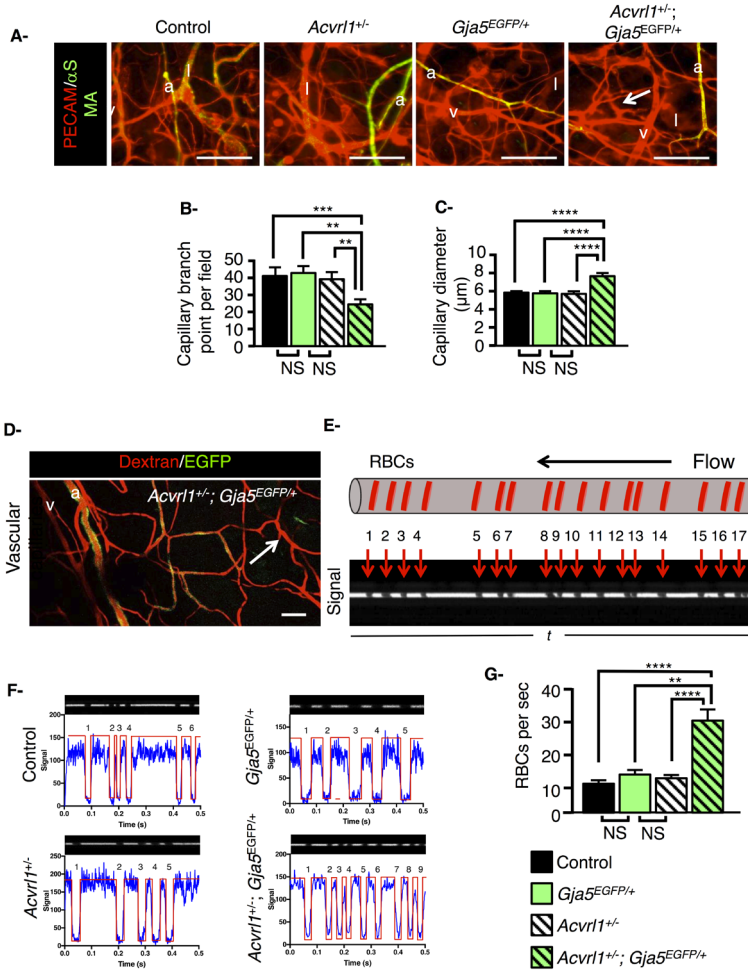

Figure 5: Measurements of RBC flow in skin capillaries of *Acvrl1*$^{+/-}$; *Gja5*$^{EGFP/+}$ mice. (A) Images of whole-mounted ears of control (n=4), *Acvrl1*$^{+/-}$ (n=5), *Gja5*$^{EGFP/+}$ (n=8) and *Acvrl1*$^{+/-}$; *Gja5*$^{EGFP/+}$ (n=12) mice stained with antibodies against PECAM-1 (endothelial cells in red) and aSMA (vSMCs in green) at P60-P90. aSMA reveals arteries. The capillary network in whole-mount images of ears reveal rarefaction of the capillary network and increased capillary diameter in *Acvrl1*$^{+/-}$; *Gja5*$^{EGFP/+}$ mice compared to control, *Acvrl1*$^{+/-}$ or *Gja5*$^{EGFP/+}$ mice. White arrows indicate increased capillary diameter. Scale bars, 200μm. **(B-C)** Quantification of the number of capillary branch points and vessel diameters. **(D)** Injection of Rhodamine B isothiocyanate-Dextran reveals capillaries in skin. The white arrow indicates an enlarged capillary directly connected to a small arteriole labeled with EGFP in *Acvrl1*$^{+/-}$; *Gja5*$^{EGFP/+}$ mice. Scale bars, 200μm. **(E)** The fluorescence of Rhodamine B isothiocyanate-Dextran in the plasma is shadowed by passing RBCs during the excitation gate. Red arrows correspond to individual RBC on the bottom. **(F)** Automatic detection of RBC transients allows local extraction of blood flow rates. **(G)** Quantification of RBC per second in capillaries of adult ears in control ($n_{capillary}$=29), *Gja5*$^{EGFP/+}$ ($n_{capillary}$=29), *Acvrl1*$^{+/-}$ ($n_{capillary}$=45) and *Acvrl1*$^{+/-}$; *Gja5*$^{EGFP/+}$ ($n_{capillary}$=34) mice. All error bars represent s.e.m. $^{*}P< 0.05$, $^{**}P< 0.01$, $^{***}P< 0.001$ and $^{****}P< 0.0001$, results from unpaired *t* test. NS, not significant, a, arteries; v, veins; l, lymphatic vessels.

Figure 6

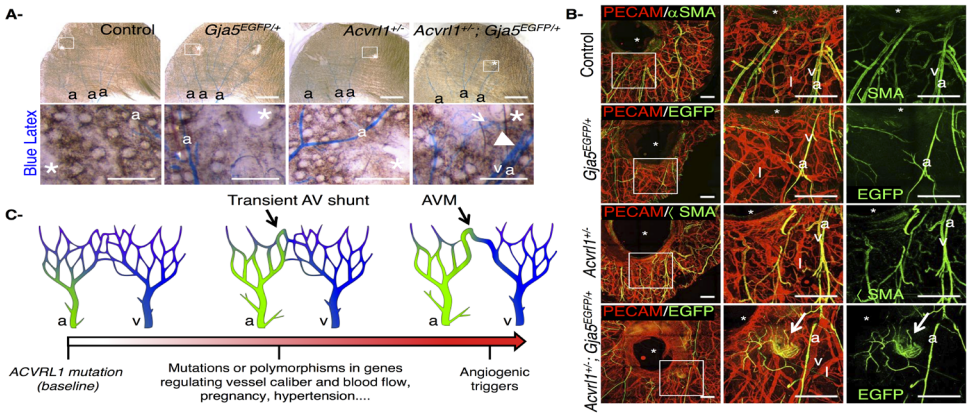

Figure 6: Wounding can induce *de novo* AVM formation in *Acvrl1*$^{+/-}$; *Gja5*$^{EGFP/+}$ mice. (A) Skin vasculature of control (n=8), *Gja5*$^{EGFP/+}$ (n=5), *Acvrl1*$^{+/-}$ (n=9) and *Acvrl1*$^{+/-}$; *Gja5*$^{EGFP/+}$ (n=7) ear shown by latex dye injection after one month of wounding. Scale bars, 1mm. Right, higher magnifications of the vascular network around the wound. Scale bars, 200µm. The development of AVM is indicated by white arrow. Note that only in *Acvrl1*$^{+/-}$; *Gja5*$^{EGFP/+}$ mutant mice developed AV shunts, revealed by the presence of blue latex in both arteries and veins as indicated in (white arrowhead). The presence of AVMs was only found in the wound area. Asterisks indicate the center of the wound. a, arteries and v, veins. **(B)** Confocal images of whole-mounted ears of 3 months old control (n=8), *Gja5a*^{EGFP} (n=5), *Acvrl1*$^{+/-}$ (n=9) and *Acvrl1*$^{+/-}$; *Gja5a*^{EGFP} (n=7) mice stained two weeks after wounding for PECAM-1 marking endothelial cells in red and for aSMA (VSMCs in green) or labeled in EGFP to identity the arteries. The white arrow indicates the formation of a system of multiple feeding arteries, the tangle or nidus and enlarged draining veins in *Acvrl1*$^{+/-}$; *Gja5a*^{EGFP}. **(C)** Working model for AVM formation in HHT2. Heterozygosity of *Acvrl1* represents the baseline situation in HHT2. The vascular network shows distinguishable arteries and veins separated by a highly branched vascular plexus. Pathological enlargement of the arterial vessels results in the delivery of more blood volume to the downstream capillaries that adapt by enlarging and by forming transient AV shunts. Sustained angiogenesis promotes further the enlargement of these AV shunts that may form large AVMs.

Discussion

In this study, we identified *Gja5* as a potential genetic modifier of AVMs in HHT2. Our work revealed that the BMP9-ALK1 signaling pathway targets *Gja5* and that reduced expression of *Gja5* in *Acvrl1* heterozygous mutants leads to arterial vasodilation and rarefaction of the post-arterial capillary network. In order to normalize the changes in hemodynamic forces and drain the engorged arterial system, capillaries become enlarged and form transient arteriovenous connections that can develop into AVMs when exposed to environmental insults (Figure 6C). Our data suggest that *Acvrl1* haploinsufficiency combined with the effects of modifier genes that regulate vessel caliber and blood flow are responsible for the heterogeneity and severity of the clinical manifestations in individuals with HHT2 and provide a novel "three hits hypothesis model" for AVM development.

Our data provide the first demonstration that changes in arterial vessel precede AVM formation in HHT mouse models and importantly, we identify *Gja5* as a potential modifier gene for HHT2. We report that the ALK1 signaling pathway stimulates the expression of *Gja5*, most importantly though BMP9. Reduced expression of *Gja5* in *Acvrl1* heterozygous mice results in enlarged arterial vessels, altered blood flow and the formation of transient AV shunts in the capillary bed; these can remodel into large AVMs where there is a pro-angiogenic and pro-inflammatory environment. Our findings are consistent with recent work showing that loss of *Acvrl1* in zebrafish embryos leads to pathological arterial enlargement and consequently altered blood flow to induce lethal AVM formation [19]. *Acvrl1*$^{+/-}$*; Gja5*$^{EGFP/+}$ double heterozygous mice provide a novel genetic model in which AVMs develop consistently and robustly. Most importantly, the AVMs resemble those seen in HHT patients, making this model an invaluable tool for uncovering the molecular and cellular defects that lead to vascular malformations in HHT, in particular those related to blood flow alterations. The *Gja5* gene encodes for Cx40, a gap junction protein expressed in the developing arterial network, starting at the onset of perfusion [37]. In the vascular system, endothelial cells predominantly express Cx37 (*Gja4)* and Cx40 whereas vascular smooth muscle cells mostly express Cx43 (*Gja1*) and Cx45 (*Gjc1*). Gap junction proteins form channels between neighboring cells to allow direct intercellular exchanges of ions and small metabolites, which are needed to coordinate vasoconstriction and vasodilation along the vessels [38, 39]. Genetic studies show that mice lacking Cx40 develop hypertension because of increased secretion of renin and reduced relaxation of peripheral vessels [40]. These defects have recently been shown to be at least partially dependent on endothelial Cx40 function indicating that Cx40 expression levels regulate blood pressure. How endothelial Cx40 controls blood pressure remains poorly understood but might be attributable to endothelial nitric oxide synthase (eNOS) activity, an important modulator of vascular tone [40]. Interestingly, both ALK1 and Cx40 interact and regulate the activity of eNOS [33, 41] suggesting that the phenotype of the *Acvrl1*$^{+/-}$*; Gja5*$^{EGFP/+}$ mice may be at least partially attributable to uncoupled eNOS activity. To support this hypothesis, we have found an increase production of ROS in the lung arteries of *Acvrl1*$^{+/-}$*; Gja5*$^{EGFP/+}$ mice. Mice carrying deletions in *Gja5* also have fewer collateral arterioles [37], whereas *Gja4*$^{-/-}$*; Gja5*$^{-/-}$ double-knockout mice die *in utero*, showing angiogenic remodeling defects with dilated blood vessels and hemorrhages [42], suggesting that Cx40 might regulate angiogenesis. Loss of *Acvrl1* expression results in excessive endothelial cell proliferation that precedes the development of AV shunts in zebrafish [19] and in *Acvrl1-iKO* mice [17]. Here, we show that reduced expression of *Gja5* in *Acvrl1* heterozygous embryos and in neonatal retinas of postnatal day 7 mice leads to significant vasodilation of the arteries

and markedly reduced numbers of post-arterial branches. In contrast to *Acvrl1*$^{+/-}$ mutant mice, we did not observe excessive endothelial proliferation in *Acvrl1*$^{+/-}$; *Gja5*$^{EGFP/+}$ mice. Defective angiogenesis may therefore be the primary event responsible for this arterial enlargement, although the mechanisms that account for this observation -decreased arterial growth, retarded migration and/or defective endothelial sprouting- remain to be elucidated. The presence of dilated arteries that deliver more blood induces the enlargement of the downstream Cx40-independent capillary-like vessels to drain this system and the formation of AV connections. This enlargement is accompanied by increased endothelial proliferation suggesting that the presence of flow stimulates further the remodeling of the capillary bed, a mechanism that might be independent of Cx40. Furthermore, loss of *Acvrl1* in zebrafish has previously been shown to result in increased expression of *cxcr4a* and decreased expression of *edn1*, suggesting that ALK1 might promote the quiescence of nascent arteries by alternative mechanisms [19]. Given the fact that these genes encode a pro-angiogenic chemokine receptor and a vasoconstrictive peptide respectively, it is logical to consider that they may regulate arterial caliber downstream of ALK1. Nevertheless, concomitant increase in *cxcr4a* and loss of *edn1* in zebrafish embryos did not copy the lack of *Acvrl1* and was not sufficient to generate AVMs [19].

Genetic polymorphisms have been detected in both promoter regions of *GJA5* and suspected to be associated with risk of cardiovascular diseases including hypertension [39]. These polymorphisms have been shown to affect *GJA5* promoter activity by reducing gene expression by approximately half with inter-assay variations ranging from 20% to 65% reduction. By comparing the expression levels of Cx40 in sections of human skin biopsies isolated from 5 healthy donors and 4 HHT2 patients, we have confirmed that important differences exist between individuals and more importantly, we reveal that Cx40 protein levels are particularly low in the majority of a small selection of HHT2 patients compared to the healthy donors supporting an association between ALK1 signaling and Cx40 expression. In conclusion, our findings provide novel insights into the mechanisms underlying AVM pathogenesis in HHT2 elicited by increased arterial caliber that might ultimately be used for drug development for HHT. Moreover, we identity *GJA5* as a potential modifier gene for HHT2 in which, genetic variations such as polymorphisms affecting “normal” expression levels are associated with disease progression.

Materials and Methods

Mice and tissues. Experiments were carried out according to the guidelines of the European Community Council Directives of January 1st 2013 (2010/63/EU) and all efforts were made to minimize the number of animals used and their suffering. The Animal Experiment Committee of Ile de France approved all protocols. The following mouse strains were used: *Cdh5-CreERT2* mice were provided by R. Adams, Max Planck Institute for Molecular Biomedicine, Münster, Germany [43]. *Acvrl1+/-* and *Acvrl1flox/flox* mice were kindly provided by Paul Oh, University of Florida, Gainesville, USA [12,17]. *Cx40EGFP/+* mice were provided by L. Miquerol, Aix Marseille University, CNRS, IBDM, UMR 7288, France [44]. Mice were maintained as heterozygotes on a mixed C56BL/6 and CD1 genetic background. *Acvrl1*fl/fl; *Cdh5-CreERT2* mice have been previously described [17]. These mice were bred with *Gja5EGFP/+* mice to generate *Acvrl1*fl/+; *Cdh5-CreERT2* and *Acvrl1*fl/+; *Cdh5-CreERT2; Gja5EGFP/+*mice. To activate CreERT2, neonatal mice were IP injected twice with 50µl oftamoxifensolution (1mg ml-1, Sigma-Aldrich, T5648) at P2 and P4, respectively. To analyze post-natal angiogenesis in the mouse retina, P7 pups were sacrificed and eyes were removed and prefixed in 4% Paraformaldehyde (PFA) in PBS for 10min at room temperature. We dissected the retinas post-fixed them in 4% PFA in PBS overnight and then processed them for immunohistochemistry as described [26]. Ear wound healing was performed as described [17]. Briefly, ears from mice at P60 were wounded using a 2mm-needle. One month later, mice were anesthetized with 2% isoflurane (Baxter S.A.S, DDG9623) and latex blue (BR80B, Connecticut, Valley Biological Supply, USA) was steadily injected into the left ventricle as previously described after dilatation with PBS-vasodilator solution containing heparin 10U/ml (Sigma-Aldrich, H3149), papaverin 0.04mg/ml (Sigma-Aldrich, P3510) and sodium nitroprusside 100mM (Sigma-Aldrich, 71778) and after fixation with PFA 4%. For whole-mount staining of cutaneous blood vessels, mice were killed 2 weeks post-wound and ears were dissected with forceps, separating the dorsal and the ventral leaflets. We fixed dorsal halves in 4% PFA overnight at 4°C and processed them as described [26].

Human material. Four HHT2 and five healthy donor skin samples were obtained from St Antonius Hospital (Department of Pulmonary Disease, Nieuwegein, The Netherlands) and Leiden University Medical Center (Department of Molecular Cell Biology, Leiden, The Netherlands) respectively following informed consent. Sections were processed as described previously [26]. Briefly, we collected skin biopsies in physiological salt, fixed them overnight in 0.2% paraformaldehyde in 0.1M phosphate buffer with 0.12 CaCl2 and 4% sucrose. We used 8µm sections for staining. We fixed frozen sections in cold acetone, washed them with PBS, blocked them with blocking reagent (Roche) and incubated them overnight at 4 °C with primary antibodies in PBS plus 0.2% BSA (A4503, Sigma). After washing, we incubated sections for 1 h at 20 °C with secondary antibodies diluted in PBS with 0.2% BSA and mounted them in DAKO mounting medium (S3023, DAKO). We captured images with a confocal laser-scanning microscope SP5 (Leica).

Antibodies and recombinant proteins. Antibody rat anti-mouse PECAM-1 (clone MEC 13.3) was purchased from BD Biosciences (553370), FITC (F3777) or Cya3- (ab7817) conjugated anti-Smooth Muscle Actin (SMA) (clone 1A4) was obtained from Sigma-Aldrich, antibody mouse anti-human PECAM-1 (IR61061) and goat anti-human Cx40 (sc-20466) were purchased from Dako and Santa Cruz Biotechnology, respectively. AlexaFluor-conjugated secondary antibodies were anti-goat alexa488 (A11055), anti-mouse alexa555

(A21422) and anti-rat555 (A21434) from Invitrogen. Nuclei were counterstained with DAPI (Invitrogen, D1306). To analyse microvasculature, mouse retinas were stained with biotinylated *Griffonia simplicifolia* lectin (isolectin B4) (B-1205) obtained from Vector Laboratories and streptavidin Cya-3 (PA43001) or Cya-5 (PA45001) from Sigma-Aldrich. Recombinant BMP9 was obtained from R&D Systems (3209-BP-010).

Immunofluorescence and DHE staining. ROS levels were assessed by dihydroethidium (DHE) staining of mouse lung sections as previously described (D-1168, Molecular Probes, Thermo Fisher). We used 7µm sections for staining. Arteries were stained with FITC (F3777) conjugated anti-Smooth Muscle Actin (SMA) (clone 1A4) obtained from Sigma-Aldrich. Whole-mount immunofluorescent staining of retinas or ears was as previously described [21, 45]. Images were captured with a confocal laser-scanning microscope SP5 (Leica), Leica DMRB, Zeiss stereo Discovery V20 microscopes or Zeiss Axio Zoom V.16.

Morphometry and quantitative analysis. We quantified branch points per field and vessel length as previously described [26]. At least three images were analyzed per mouse. For density, we measured the total cellular area (pixels) by converting compressed Z-stacks to black and white followed by manual threshold adjustment to highlight cell contours. Cell surface area was quantified with ImageJ software (US National Institute of Health). Vessel diameter was measured using PECAM-1 (+) compressed Z-stack images from similar regions in the ear using ImageJ. Digital images of human skin sections were acquired with a Leica SP5 confocal microscope. ImageJ software was used for computerized analysis of immunostained vascular structures. The images were fixed at threshold intensity, values below being excluded from analysis. For each image, vessel surface was defined as PECAM (+) pixels and determined by the total grey value. In the corresponding Cx40 image, fluorescence intensity was calculated with the integrated intensity defined as the sum of all pixels in the image. Cx40 fluorescence intensity was defined as the ratio of Cx40 integrated intensity to PECAM total grey value of at least 5 independent images for each individual.

Cell culture and transfection. Human Arterial Endothelial Cells (HuAECs) were obtained as described [45] and cultured in EGM-M2 SupplementPack (PromoCell, C-39211) at 37°C in 5% CO2. Cells were washed with phosphate-buffered saline (PBS) (Gibco, 14200-067) and then serum-starved for 5 hours prior to stimulation with either 1ng/ml for 3h or 10ng/ml BMP9 for 24h to assess the effect of BMP9 on gene expression.
HuAECs were transfected either with siRNA control (AllStars negative control, 11175471, Qiagen) or siRNA targeting human *ACVRL1* (FlexiTube siRNA SI02758392, Qiagen). Transfections were carried out at a final concentration of 5nM in 12-well plates using OligofectamineTransfection Reagent (12252-011, Invitrogen) overnight and then medium was changed.

Protein extraction and western blot analysis. Cell lysates were prepared with RIPA buffer (50mM Tris-HCl, 250mM NaCl, 2% NonidentP40, 2.5mM EDTA-Na, 0.1% SDS, 0.5% DOC, pH 7.2) containing complete protease inhibitor cocktail II (Roche Applied Science). Protein concentrations were determined using the DC Protein Assay Kit II (BioRad). Samples were analyzed by Western blot using 10% polyacrylamide gels, followed by overnight wet-transfer of the proteins to activated nitrocellulose membranes Hybond-C Extra (Amersham, Biosciences). Membranes were blocked in TBS-T (0.01 M Tris-HCl, pH 7.4,

0.15M NaCl, 0.1% Tween-20) with 5% dried milk and incubated overnight with the indicated antibodies. Signal detection was performed using the ECL system and SuperSignal West Pico Chemiluminecent Substrate (Thermo Scientific). The antibodies used in the study are the following: anti-pSMAD1/5 (1:1000, Cell Signaling Technology, Danvers, MA, USA), SMAD1/5 antibody (1:1000, Santa Cruz, SC-6031), anti-GAPDH (1:1000, Sigma), HRP-conjugated secondary antibodies IgG(1:5000, Cell Signaling).

Quantitative PCR analysis. RNA was isolated from HuAECs using the RNeasy Mini Kit (QIAGEN, 74104). *In vitro* reactions were performed from every RNA sample using Superscript III Reverse Transcriptase first-Strand Synthesis Kit for real-time (RT)-PCR (Invitrogen, 18080-044). RNA extracted was quantified using a Biomate 3 Spectrophotometer. Quantitative PCR (MyiQ Single Color Real-Time Detection System, Bio-Rad) was performed in duplicate using the MyIQTM real-time PCR system (Biorad). Each 20ml contained 200ng of cDNA, 10ml iQTM SYBR® Green Supermix (Biorad, 1708880), 250nM of forward and reverse primers and nuclease free water. Primers used were as followed: *GJA5* (Forward primer 5'- AATCAGTGCCTGGAGAATGG-3', reverse primer 5'CGAACCTGGATGAAACCTTC-3'), *HEY2* (Forward primer 5'-GATTCAGCCCTCCGAATG-3', reverse primer 5' TGGCAGAGAGGGACAAGAG-3'), *ID1* (Forward primer 5'-TGTCTGTCTGAGCAGAGCGT- 3', reverse primer 5'-TAGTCGATGACGTGCTGGAG-3') and the human reference genes *GAPDH* (QIAGEN, QT01192646) and *ACTB* (QIAGEN, QT00095431) for normalization. Quantitative PCR was performed with an initial denaturation step of 15min at 95oC followed by 40 cycles of 15s denaturation at 95oC, 30s annealing at 58oC, and 30s extension at 72oC. Four biological replicates were carried out for all quantitative PCR reactions.

Vasomotion and Red blood cell flow analysis. Adult mice were anesthetized by inhalation of isofluorane 2% (Baxter S.A.S, DDG9623). 100ml of Fluorescence Rhodamine B isothiocyanate-Dextran (Sigma-Aldrich, R9379- 250MG) was retro-orbitally injected. After 3min, the selecting points of interest in the arterial vessels or in the capillaries were captured by fast fluorescence-based scanning using 25x objective (HCX IRAPO L 25x/0.95 W). We have recorded spontaneous vasodilation and vasoconstriction of the arterial vessels at 1Hz during 100s. The relation between vessel diameter and a vasomotion index is defined as the area under the curve for percent spontaneous changes in vessel diameter with a ±5% cutoff threshold. We have also measured short transients in the PMT signal collected during xt phase at 1.4MHz for 20 seconds in each capillary vessel as previously described [35]. Red blood cells (RBCs) appeared as dark shadows on bright red background because of the Dextran contained in the blood plasma. Importantly, when the diameter of the vessel allowed passage of RBCs only in single file, as in the case of capillaries, the flux of RBCs is simply the number of RBCs that pass per second [35].

Electrostimulation. Electrostimulation of the retinal arteries was performed as described [46,47] . Briefly, whole retina were mounted and maintained in an extracellular solution (37 °C) (NaCl 140 mM; Glucose 25 mM; KCl 5.5 mM; CaCl2 1.8 mM; MdCl2 1 mM; Hepes 10 mM; ph = 7.3)). On whole mounted retinas, vascular smooth muscle cells were patched with pipette filed with the same solution. Resistance of the pipette was measured before each experiment in order to define the input voltage (pulses 0.02 ms, 10 Hz for 5 s) to be applied so as to deliver a current intensity increasing from 1 to 4μA. Vascular smooth muscle cells

were stimulated by applying voltage pulses 20 seconds after the patch. A total of 300 images was recorded in 2.5min.

BrdU staining in P7 retina. To investigate endothelial cell proliferation, P7 pups were injected subcutaneously with 250µg of BrdU per gram body weight 3 hours before euthanasia. Retinas were subjected to antigen retrieval with 2N HCl and 1%Triton, washed with 0.1M Tris-HCl pH8 and stained with mouse anti-BrdU (1:500, Sigma-Aldrich, B8434). Secondary Alexa Fluor555 anti-mouse IgG1 (Life Technologies, 1:250) was used to detect primary anti-BrdU antibody.

Whole E12.5 embryo staining. E12.5 mouse embryos were isolated and fixed in 4% paraformaldehyde for 3 hours. Washed with TNT solution (10%Tris pH7.4, 0.15M NaCl and 0.05% Tween) and permeabilized in PBS with 0.3% Triton. Embryos were then incubated in blocking buffer TNBT (10%Tris pH7.4, 0.15M NaCl, 0.5% Perkin Elmer blocking and 0.5% Triton X100) overnight at 4°C. Vasculature was stained with primary rat anti-mouse CD31 antibody (BD Pharmingen Clone: MEC 13.3, 1:100) for 2 days and secondary Alexa Fluor555 anti-rat (BD Biosciences, 1:250) overnight at 4°C.

Statistical Analysis. We performed statistical analyses with Prism 6 software (GraphPad) using one-way Anova analysis the mean of three or more independent groups and using the two-tailed, unpaired Student's *t* test. Data were expressed as mean ±SEM. $P< 0.05$ was considered to be statistically significant.

References

1. Shovlin CL. Hereditary haemorrhagic telangiectasia: pathophysiology, diagnosis and treatment. *Blood reviews*. 2010;24:203-19.
2. McAllister KA, Grogg KM, Johnson DW, *et al.* Endoglin, a TGF-beta binding protein of endothelial cells, is the gene for hereditary haemorrhagic telangiectasia type 1. *Nature genetics*. 1994;8:345-51.
3. Johnson DW, Berg JN, Baldwin MA, *et al.*. Mutations in the activin receptor-like kinase 1 gene in hereditary haemorrhagic telangiectasia type 2. *Nature genetics*. 1996;13:189-95.
4. Lebrin F, Goumans MJ, Jonker L, Carvalho RL, Valdimarsdottir G, Thorikay M, Mummery C, Arthur HM and ten Dijke P. Endoglin promotes endothelial cell proliferation and TGF-beta/ALK1 signal transduction. *The EMBO journal*. 2004;23:4018-28.
5. David L, Mallet C, Mazerbourg S, Feige JJ and Bailly S. Identification of BMP9 and BMP10 as functional activators of the orphan activin receptor-like kinase 1 (ALK1) in endothelial cells. *Blood*. 2007;109:1953-61.
6. Lebrin F, Deckers M, Bertolino P and Ten Dijke P. TGF-beta receptor function in the endothelium. *Cardiovascular research*. 2005;65:599-608.
7. McDonald J, Bayrak-Toydemir P and Pyeritz RE. Hereditary hemorrhagic telangiectasia: an overview of diagnosis, management, and pathogenesis. *Genetics in medicine : official journal of the American College of Medical Genetics*. 2011;13:607-16.
8. Leblanc GG, Golanov E, Awad IA, Young WL and Biology of Vascular Malformations of the Brain NWC. Biology of vascular malformations of the brain. *Stroke; a journal of cerebral circulation*. 2009;40:e694-702.
9. Braverman IM, Keh A and Jacobson BS. Ultrastructure and three-dimensional organization of the telangiectases of hereditary hemorrhagic telangiectasia. *The Journal of investigative dermatology*. 1990;95:422-7.
10. Tual-Chalot S, Oh SP and Arthur HM. Mouse models of hereditary hemorrhagic telangiectasia: recent advances and future challenges. *Frontiers in genetics*. 2015;6:25.
11. Bourdeau A, Dumont DJ and Letarte M. A murine model of hereditary hemorrhagic telangiectasia. *The Journal of clinical investigation*. 1999;104:1343-51.
12. Srinivasan S, Hanes MA, Dickens T, Porteous ME, Oh SP, Hale LP and Marchuk DA. A mouse model for hereditary hemorrhagic telangiectasia (HHT) type 2. *Human molecular genetics*. 2003;12:473-82.
13. Torsney E, Charlton R, Diamond AG, Burn J, Soames JV and Arthur HM. Mouse model for hereditary hemorrhagic telangiectasia has a generalized vascular abnormality. *Circulation*. 2003;107:1653-7.
14. Xu B, Wu YQ, Huey M, Arthur HM, Marchuk DA, Hashimoto T, Young WL and Yang GY. Vascular endothelial growth factor induces abnormal microvasculature in the endoglin heterozygous mouse brain. *Journal of cerebral blood flow and metabolism : official journal of the International Society of Cerebral Blood Flow and Metabolism*. 2004;24:237-44.
15. Hao Q, Zhu Y, Su H, Shen F, Yang GY, Kim H and Young WL. VEGF Induces More Severe Cerebrovascular Dysplasia in Endoglin than in Alk1 Mice. *Translational stroke research*. 2010;1:197-201.
16. Li C, Guo B, Ding S, Rius C, Langa C, Kumar P, Bernabeu C and Kumar S. TNF alpha down-regulates CD105 expression in vascular endothelial cells: a comparative study with TGF beta 1. *Anticancer research*. 2003;23:1189-96.
17. Park SO, Wankhede M, Lee YJ, Choi EJ, Fliess N, Choe SW, Oh SH, Walter G, Raizada MK, Sorg BS and Oh SP. Real-time imaging of de novo arteriovenous malformation in a mouse model of hereditary hemorrhagic telangiectasia. *The Journal of clinical investigation*. 2009;119:3487-96.
18. Mahmoud M, Allinson KR, Zhai Z, Oakenfull R, Ghandi P, Adams RH, Fruttiger M and Arthur HM. Pathogenesis of arteriovenous malformations in the absence of endoglin. *Circulation research*. 2010;106:1425-33.
19. Corti P, Young S, Chen CY, Patrick MJ, Rochon ER, Pekkan K and Roman BL. Interaction between alk1 and blood flow in the development of arteriovenous malformations. *Development*. 2011;138:1573-82.
20. Laux DW, Young S, Donovan JP, Mansfield CJ, Upton PD and Roman BL. Circulating Bmp10 acts through endothelial Alk1 to mediate flow-dependent arterial quiescence. *Development*. 2013;140:3403-12.
21. Larrivee B, Prahst C, Gordon E, del Toro R, Mathivet T, Duarte A, Simons M and Eichmann A. ALK1 signaling inhibits angiogenesis by cooperating with the Notch pathway. *Developmental cell*. 2012;22:489-500.
22. de Wit C, Roos F, Bolz SS, Kirchhoff S, Kruger O, Willecke K and Pohl U. Impaired conduction of vasodilation along arterioles in connexin40-deficient mice. *Circulation research*. 2000;86:649-55.
23. Figueroa XF, Paul DL, Simon AM, Goodenough DA, Day KH, Damon DN and Duling BR. Central role of connexin40 in the propagation of electrically activated vasodilation in mouse cremasteric arterioles in vivo. *Circulation research*. 2003;92:793-800.
24. Milkau M, Kohler R and de Wit C. Crucial importance of the endothelial K+ channel SK3 and connexin40 in arteriolar dilations during skeletal muscle contraction. *FASEB journal : official publication of the Federation*

of American Societies for Experimental Biology. 2010;24:3572-9.
25. Vorderwulbecke BJ, Maroski J, Fiedorowicz K, Da Silva-Azevedo L, Marki A, Pries AR and Zakrzewicz A. Regulation of endothelial connexin40 expression by shear stress. *American journal of physiology Heart and circulatory physiology*. 2012;302:H143-52.
26. Lebrin F, Srun S, Raymond K, *et al*. Thalidomide stimulates vessel maturation and reduces epistaxis in individuals with hereditary hemorrhagic telangiectasia. *Nature medicine*. 2010;16:420-8.
27. Meysen S, Marger L, Hewett KW, Jarry-Guichard T, Agarkova I, Chauvin JP, Perriard JC, Izumo S, Gourdie RG, Mangoni ME, Nargeot J, Gros D and Miquerol L. Nkx2.5 cell-autonomous gene function is required for the postnatal formation of the peripheral ventricular conduction system. *Developmental biology*. 2007;303:740-53.
28. Tual-Chalot S, Mahmoud M, Allinson KR, Redgrave RE, Zhai Z, Oh SP, Fruttiger M and Arthur HM. Endothelial depletion of Acvrl1 in mice leads to arteriovenous malformations associated with reduced endoglin expression. *PloS one*. 2014;9:e98646.
29. Bernabeu MO, Jones ML, Nielsen JH, Kruger T, Nash RW, Groen D, Schmieschek S, Hetherington J, Gerhardt H, Franco CA and Coveney PV. Computer simulations reveal complex distribution of haemodynamic forces in a mouse retina model of angiogenesis. *Journal of the Royal Society, Interface / the Royal Society*. 2014;11.
30. Park SO, Lee YJ, Seki T, Hong KH, Fliess N, Jiang Z, Park A, Wu X, Kaartinen V, Roman BL and Oh SP. ALK5- and TGFBR2-independent role of ALK1 in the pathogenesis of hereditary hemorrhagic telangiectasia type 2. *Blood*. 2008;111:633-42.
31. Wang Y, Nakayama M, Pitulescu ME, Schmidt TS, Bochenek ML, Sakakibara A, Adams S, Davy A, Deutsch U, Luthi U, Barberis A, Benjamin LE, Makinen T, Nobes CD and Adams RH. Ephrin-B2 controls VEGF-induced angiogenesis and lymphangiogenesis. *Nature*. 2010;465:483-6.
32. Looft-Wilson RC, Billaud M, Johnstone SR, Straub AC and Isakson BE. Interaction between nitric oxide signaling and gap junctions: effects on vascular function. *Biochimica et biophysica acta*. 2012;1818:1895-902.
33. Jerkic M, Kabir MG, Davies A, Yu LX, McIntyre BA, Husain NW, Enomoto M, Sotov V, Husain M, Henkelman M, Belik J and Letarte M. Pulmonary hypertension in adult Alk1 heterozygous mice due to oxidative stress. *Cardiovascular research*. 2011;92:375-84.
34. Jerkic M and Letarte M. Contribution of oxidative stress to endothelial dysfunction in hereditary hemorrhagic telangiectasia. *Frontiers in genetics*. 2015;6:34.
35. Lecoq J, Parpaleix A, Roussakis E, Ducros M, Goulam Houssen Y, Vinogradov SA and Charpak S. Simultaneous two-photon imaging of oxygen and blood flow in deep cerebral vessels. *Nature medicine*. 2011;17:893-8.
36. Garrido-Martin EM, Nguyen HL, Cunningham TA, Choe SW, Jiang Z, Arthur HM, Lee YJ and Oh SP. Common and distinctive pathogenetic features of arteriovenous malformations in hereditary hemorrhagic telangiectasia 1 and hereditary hemorrhagic telangiectasia 2 animal models--brief report. *Arteriosclerosis, thrombosis, and vascular biology*. 2014;34:2232-6.
37. Buschmann I, Pries A, Styp-Rekowska B, *et al.* Pulsatile shear and Gja5 modulate arterial identity and remodeling events during flow-driven arteriogenesis. *Development*. 2010;137:2187-96.
38. Haefliger JA, Nicod P and Meda P. Contribution of connexins to the function of the vascular wall. *Cardiovascular research*. 2004;62:345-56.
39. Molica F, Meens MJ, Morel S and Kwak BR. Mutations in cardiovascular connexin genes. *Biology of the cell / under the auspices of the European Cell Biology Organization*. 2014;106:269-93.
40. Morton SK, Chaston DJ, Howitt L, Heisler J, Nicholson BJ, Fairweather S, Broer S, Ashton AW, Matthaei KI and Hill CE. Loss of functional endothelial connexin40 results in exercise-induced hypertension in mice. *Hypertension*. 2015;65:662-9.
41. Le Gal L, Alonso F, Mazzolai L, Meda P and Haefliger JA. Interplay between connexin40 and nitric oxide signaling during hypertension. *Hypertension*. 2015;65:910-5.
42. Simon AM and McWhorter AR. Vascular abnormalities in mice lacking the endothelial gap junction proteins connexin37 and connexin40. *Developmental biology*. 2002;251:206-20.
43. Pitulescu ME, Schmidt I, Benedito R and Adams RH. Inducible gene targeting in the neonatal vasculature and analysis of retinal angiogenesis in mice. *Nature protocols*.2010;5:1518-34.
44. Miquerol L, Bellon A, Moreno N, Beyer S, Meilhac SM, Buckingham M, Franco D and Kelly RG. Resolving cell lineage contributions to the ventricular conduction system with a Cx40-GFP allele: a dual contribution of the first and second heart fields. Developmental dynamics : an official publication of the American Association of Anatomists.2013;242:665-77.
45. Luu NT, Rahman M, Stone PC, Rainger GE and Nash GB. Responses of endothelial cells from different vessels to inflammatory cytokines and shear stress: evidence for the pliability of endothelial phenotype. Journal of vascular research. 2010;47:451-61.

46. Peppiatt CM, Howarth C, Mobbs P and Attwell D. Bidirectional control of CNS capillary diameter by pericytes. Nature. 2006;443:700-4.
47. Mishra A, O'Farrell FM, Reynell C, Hamilton NB, Hall CN and Attwell D. Imaging pericytes and capillary diameter in brain slices and isolated retinae. Nature protocols.2014;9:323-36.

Supplementary Figures

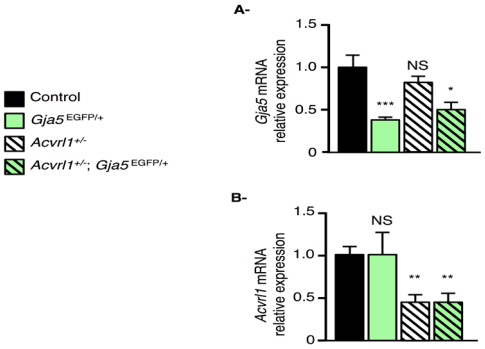

Figure I: *Gja5* and *Acvrl1* mRNA expression levels in control, *Gja5EGFP/+*, *Acvrl1+/-* and *Acvrl1+/-; Gja5EGFP/+* mice. (A-B) Graphs showing relative expression levels of *Gja5* **(A)** and *Acvrl1* **(B)** mRNA isolated from P7 retinas. Error bars represent s.e.m. **P*< 0.05, ***P*< 0.01, ****P*< 0.001 result from unpaired *t* test. NS, not significant.

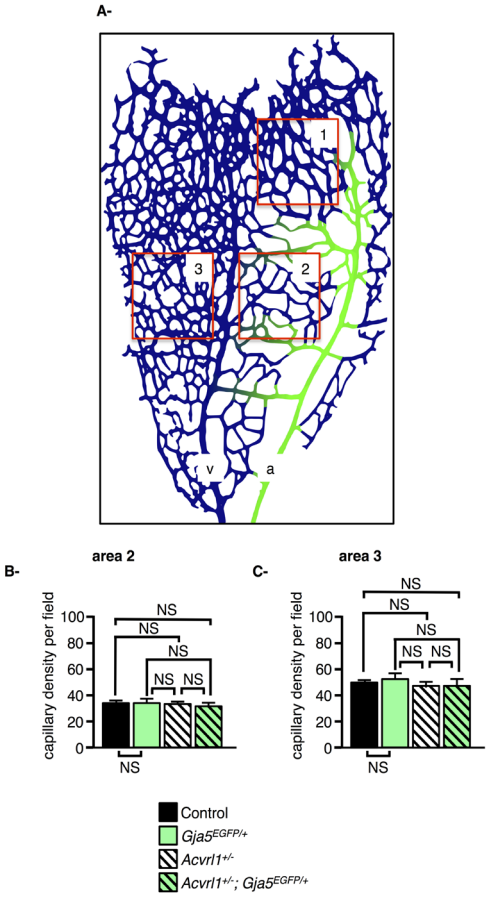

Figure II: Vascular network density analysis related to the distribution of hemodynamic forces in P7 mouse retina. (A) Scheme of the distribution of the hemodynamic forces as generated by computation methods. Vessels with preferential high blood flow are labeled in green and correlate with arteries and with areas where advanced state of pruning are typically found at P7. The outlined red boxes indicate the areas in which vascular parameters were quantified. *Acvrl1+/-; Gja5EGFP/+* mutant mice show reduced capillary density in post-arterial vessels of the vascular front (area 1) compared to control, *Gja5EGFP/+* or *Acvrl1+/-* mice. **(B-C)** Quantification of the capillary density in area 2 **(B)** and in area 3 **(C)** of control (n= 9), *Gja5EGFP/+* (n= 8), *Acvrl1+/-* (n= 9) and *Acvrl1+/-; Gja5EGFP/+* (n= 7). Error bars represent s.e.m. *P* results from unpaired *t* test. NS, not significant.

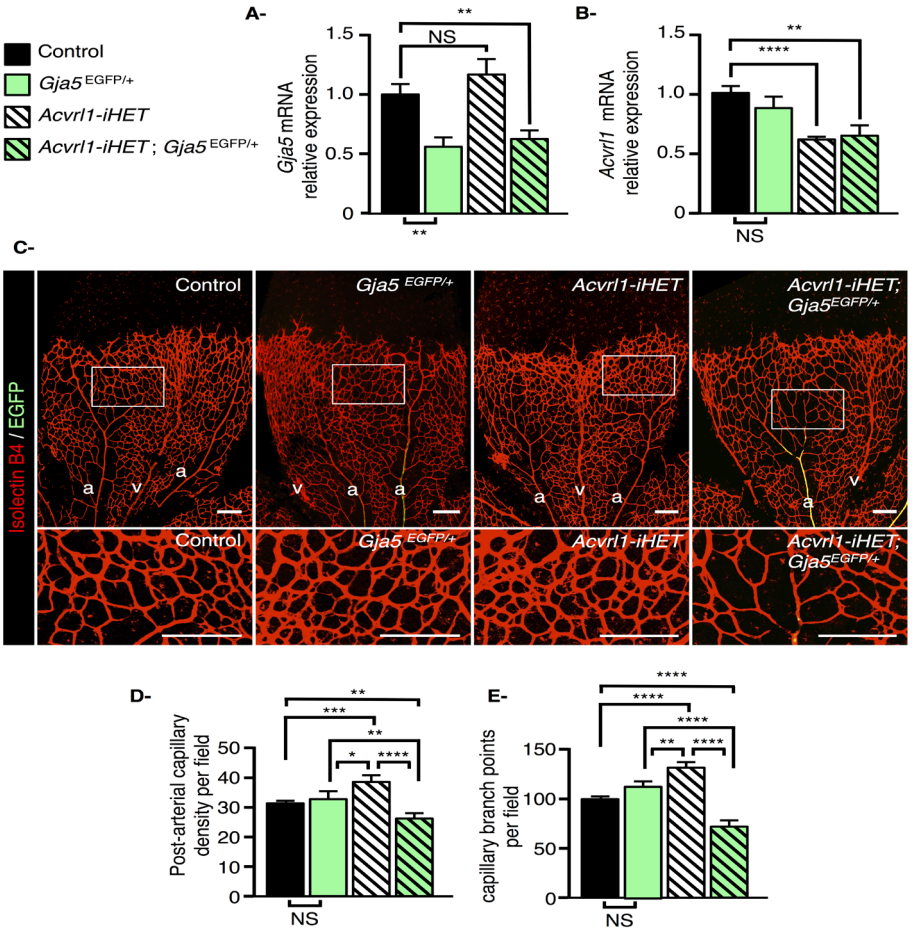

Figure III: (A-B) Effect of reduced expression of *Gja5* in *Acvrl1-iHET* mouse model. Graphs showing relative expression levels of *Gja5* **(A)** and *Acvrl1* **(B)** in the retina P7 of control, *Gja5EGFP/+; Acvrl1-iHET* and *Acvrl1-iHET; Gja5EGFP/+* pups injected intraperitoneally twice at P2 and P4 with 50µg of Tamoxifen. Effect of reduced expression of *Gja5* in *Acvrl1-iHET* mouse model. **(C)** Top, Isolectin B4-stained endothelial cells in retinal vessels in control (n=12), *Gja5*EGFP/+ (n=11), *Acvrl1-iHET* (n=12) and *Acvrl1-iHET*; *Gja5*EGFP/+ (n=14) mice at P7. Bottom: higher magnifications of the post-arterial capillary plexus shown in the top row. Outlined boxes indicate the areas in which vascular parameters were quantified. **(D-E)** Quantification of post arterial capillary density **(D)** and quantification of the number of vessel branch points **(E)** per field. All error bars represent s.e.m. **P*< 0.05, ***P*< 0.01, ****P*< 0.001 and *****P*< 0.0001, result from unpaired *t* test. NS, not significant a, arteries; v, veins. Scale bars, 200µm.

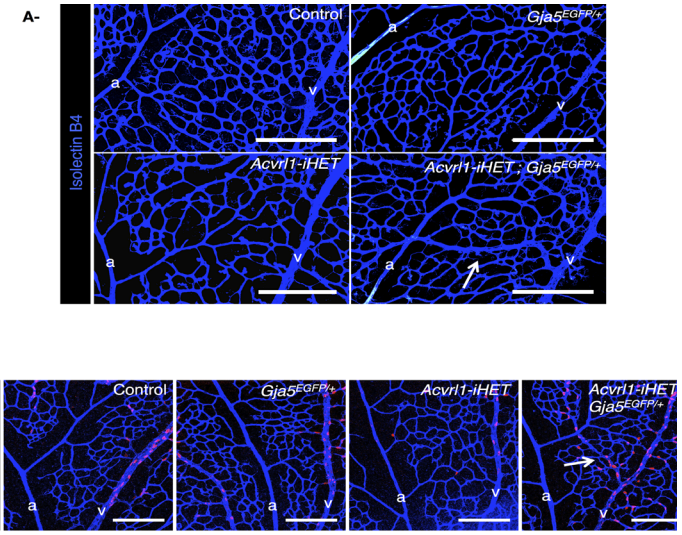

Figure IV: Development of transient AV connections in *Acvrl1-iHET*; *Gja5*EGFP/+ neonatal retina. (A) Confocal images of flat-mounted retinas labeled with isolectin-B4 show the vascular plexus of control (n=12), *Gja5*EGFP/+ (n=9), *Acvrl1-iHET* (n=11) and *Acvrl1-iHET*; *Gja5*EGFP/+ (n=13) at P7. The white arrow indicates a direct connection between an artery and vein. **(B)** The development of an AVM shunt in *Acvrl1-iHET*; *Gja5*EGFP/+ P7 retinas is characterized by increased proliferation indicated by BrdU staining. Scale bars, 200µm

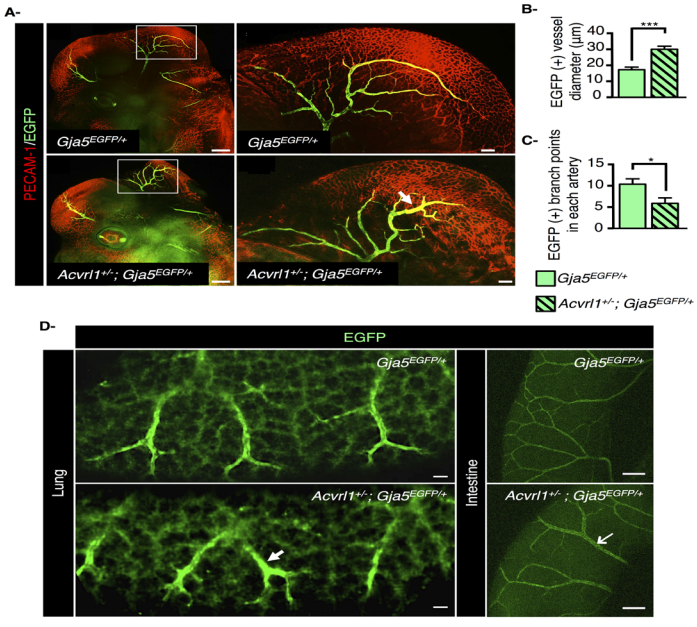

Figure V: Effect of reduced expression of *Gja5* in *Acvrl1+/-* mutant mice during embryonic development. (A) Left, PECAM-1-stained endothelial cells in E12.5 *Gja5*EGFP/+ (n=5) and *Acvrl1*+/-; *Gja5*EGFP/+ (*n* =5) embryos. Right: higher magnifications of the mesenchephalic artery from the images on the left. Scale bars 100µm. **(B)** Quantification of the arterial diameter and **(C)** quantification of the number of branch points of the EGFP (+) arteries. **(D)** Increased arterial diameter in E17.5 lung and intestine of *Acvrl1*+/-; *Gja5EGFP/*+ mice compared to *Gja5EGFP/*+ mice shown by imaging the EGFP (+) arterial network. Scale bars 200µm